ELSEVIER

Journal of Nuclear Materials 313–316 (2003) 796–803

journal of nuclear materials

www.elsevier.com/locate/jnucmat

# Theoretical understanding of turbulent transport in the SOL

Y. Sarazin [a,*], Ph. Ghendrih [a], G. Attuel [a], C. Clément [a], X. Garbet [a], V. Grandgirard [a], M. Ottaviani [a], S. Benkadda [b], P. Beyer [b], N. Bian [b], C. Figarella [b]

[a] *Association Euratom-CEA, CEA/DSM/DRFC Cadarache, 13108 Saint-Paul-lez-Durance, France*
[b] *UMR 6633 PIIM, CNRS-Université de Provence, 13397 Marseille, France*

**Abstract**

Turbulence in the scrape-off layer (SOL) is investigated using a 2D fluid model for the interchange instability as a paradigm. A constant driving flux governs the dynamics of both the equilibrium and fluctuating parts of the density and electric potential. The turbulent flux exhibits intermittent bursts, called avalanches. These events account for a significant part of the total transport, and are manifested as poloidally localized density fingers, extending towards the far SOL. The time averaged density profile looks exponential, and the SOL width increases weakly with the driving source (scaling exponent 2/9). Viscosity is found to govern the characteristic radial size of convective cells, which in turn control the transport magnitude. The larger $\nu$, the larger the turbulent transport. Finally, the impact on turbulence of local biasing is investigated, possibly modeling Langmuir probe measurements. For a too large extent of the theoretical probe, the density drops by factors at the probe, due to the local build up of a screening vortex. The ambient density is recovered for a sufficiently small probe. In this case, fluctuations exhibit a similar Fourier spectrum at and next to the probe, though the probe still misses a significant number of large bursts. Finally, the experimental probe characteristics are recovered qualitatively when varying the biasing potential.


*PACS:* 52.55.Fa, 52.35.Ra, 52.65.Kj
*Keywords:* Turbulence; Transport; Avalanches; Simulations; SOL physics; Langmuir probe measurements

## 1. Introduction

As for the core plasma, it is well known that turbulent transport plays an important role in the plasma scrape-off layer (SOL) since it governs the cross-field transport. In particular, the SOL width is generally understood as characterizing the balance between parallel transport and cross-field transport [1]. As a consequence, the SOL width is such that it is equally distant from the last closed magnetic surface via cross-field transport as from the wall via parallel transport. From this picture, cross-field transport is dominant within the first e-folding length of the SOL. Although this region of the plasma is particularly suited to investigate SOL turbulence with probe measurements [2], there is still a significant gap to fill in order to bridge the SOL modeling to the turbulence measurements. In fact, the problem of cross-field transport also interferes with the Langmuir probe measurements themselves [3]. Last but not least, the SOL width governed by the cross-field transport plays a crucial role in the design of next step devices due to the very large power handled in these devices. As such, accurate values and an extrapolation law are badly needed. Unfortunately the attempts in that direction have not been successful. More worrisome, recent data seem to indicate the existence of still narrower SOL widths [4]. Theoretical investigation is clearly needed to step forward with this complex problem.

* Corresponding author. Tel.: +33-442 25 48 03; fax: +33-442 25 62 33.
*E-mail address:* yanick.sarazin@cea.fr (Y. Sarazin).

0022-3115/03/$ - see front matter 
PII: S0022-3115(02)01437-X

A significant change in the analysis of plasma turbulence has taken place as the drive of the system was considered to be a flux rather than a gradient. Indeed, the standard analysis of systems out of thermodynamical equilibrium aims at determining the flux resulting from an imposed gradient. The latter characterizes the 'distance' from the thermodynamical equilibrium. Let us consider the density field and hence the relationship between the particle flux and density. In all fusion plasmas, the system is driven away from equilibrium by the particle injection rate and particle recycling. As such, our systems are flux driven rather than gradient driven. This change in driving force leads to significant modifications in the dynamics of the turbulent response, with continuous reorganization of the turbulent eddies and locally, repeated evolution from the linear stage to the non-linear saturation of the turbulence.

In addition to this change in approach, the interest in the poloidal flows self generated by the turbulence has increased [5] since these flows, and especially the zonal flows (ZFs), seem to play a major role in the non-linear saturation of turbulence [6]. As a result of these two inputs, turbulent models exhibit intermittent behavior with avalanche-like propagation – related to front propagation [7] and/or streamers [8] – and a large variety of dynamics, as predicted theoretically [9]. This behavior is observed in numerous fluid models for edge and core turbulence [10–13], and has also been tackled for SOL turbulence [14]. Experimental evidence of large scale transport is also reported [15].

In the present paper, we address issues that are at the crux of present experimental investigation of the SOL. In Section 2, we review the status of the 2D fluid model that is used. Turbulence is shown to generate intermittent and poloidally localized density fingers, extending much farther than the SOL e-folding length. Viscosity is found to govern the characteristic radial size of convective cells, which in turn control the transport magnitude. The exact role of ZFs in this shearing process is still to be determined. Finally, the turbulence response to probe biasing is studied in Section 3.

## 2. Interchange instability in the SOL

Fluid turbulence studies in the SOL usually make two main assumptions [17,19,20]. On the one hand, the pre-sheath is dominated by flute-like modes, characterized by almost vanishing parallel wave numbers $k_\parallel \approx 0$, making the problem 2D. More precisely, for a SOL between two toroidal limiters located at symmetrical poloidal angles $\pm\Delta\theta$, the modes are such that $k_\parallel = 2/L_\parallel = 1/qR_0\Delta\theta$. Such an approximation agrees well with experimental measurements of the turbulence parallel correlation length [16]. On the other hand, a Bohm criterion is used for sheath boundary conditions: ion parallel current losses are given by the saturation current $j_{\parallel i} = j_{sat} \equiv enc_s$, while electrons are assumed adiabatic $j_{\parallel e} \equiv -j_{sat}\exp(\Lambda - eU/T_e)$. The floating potential $\Lambda = \frac{1}{2}\ln[4T_e/(\pi(T_i + T_e))(m_i/m_e)]$ which develops at the sheath, is governed by the difference between electron and ion inertia. In steady state and in the absence of any biasing, the Bohm criterion ensures a vanishing current at the end points of the field lines, and hence $\phi \equiv eU/T_e = \Lambda$.

There exist basically two main instabilities in the SOL making use of these assumptions, namely interchange and negative sheath resistivity, sometimes referred to as the electron temperature driven instability. In the latter case, fluctuations of the parallel current are driven by electron temperature fluctuations via the Bohm constraint: $\tilde{j}_\parallel \approx -j_{sat}\Lambda\tilde{T}_e/\overline{T}_e$ [17]. These fluctuations become unstable due to the positive feedback of the fluctuating parallel electric field developing at the sheath $\tilde{E}_\parallel \approx \tilde{T}_e/e\lambda_D$, where $\lambda_D$ is the Debye length. The radial temperature gradient in the SOL then provides a reservoir of free energy to the system. The linear growth rate is typically $\gamma_{NSR} \approx c_s/\sqrt{L_\parallel L_{T_e}}(\Lambda/k_\perp\rho_s)^{1/2}$, where $\rho_s = c_s/\Omega_s$, $\Omega_s = eB/m_i$ and $c_s = (T_e/m_i)^{1/2}$. These modes are unconditionally unstable (no threshold), are not ballooned, and are studied numerically in [18].

Interchange electrostatic modes are destabilized in the SOL by the low sheath conductivity $\sigma_\parallel = \rho_s/L_\parallel$. These modes are driven by the pressure gradient in the bad curvature – low field side – region [19,20]. The instability mechanism is analogous to Rayleigh–Bénard in fluid mechanics, the average field line curvature $g = [(1+s)\sin\Delta\theta - s\Delta\theta\cos\Delta\theta]2q\rho_s/L_\parallel$ standing for the gravity field acting along the radial direction. In the limit of cold ions, $\sigma_\parallel$ and dissipative coefficients $D$ and $\nu$ (diffusion and viscosity) provide damping at low and large wave numbers respectively, leading to an instability threshold $\kappa \approx \sigma_\parallel D\nu/\rho_s R(D+\nu)$ ($D$ and $\nu$ being normalized to the Bohm coefficient $\rho_s c_s$). The growth rate is roughly given by $\gamma_{int} \approx v_{thi}/\sqrt{g/RL_n - \kappa}$.

Both linear growth rates are of the same order of magnitude for typical edge plasma parameters. Note that strong density $\tilde{n}$ and electric potential $\tilde{\phi}$ fluctuations are observed experimentally in the SOL of fusion devices, accounting for the anomalous heat transport [21]. The present paper only considers interchange modes in the 2D limit. The work focuses on the impact of profile relaxation mechanisms on the dynamics of turbulent transport. Especially, it is shown that a simple 'paradigm' model for turbulent transport in the SOL exhibits striking qualitative agreement with experiments, and allows for a reconciliation of measurements and theory.

### 2.1. Flux driven 2D model

Assuming a constant electron temperature $T_e$ and cold ions yields two parameters: the normalized sheath

conductivity $\sigma_\parallel$ and the parallel average of the field line curvature $g$. The normalized system is then derived from particle and charge conservation laws [14]:

$$\begin{aligned} &\mathrm{d}/\mathrm{d}tn = -\sigma_\parallel n \exp(\Lambda - \phi) + D\nabla_\perp^2 n + S, \\ &\frac{\mathrm{d}}{\mathrm{d}t}\nabla_\perp^2 \phi = \sigma_\parallel\{1 - \exp(\Lambda - \phi)\} - g\partial_y \mathrm{Log}(n) + \nu\nabla_\perp^4 \phi, \end{aligned} \tag{1}$$

where the total time derivative stands for the Lagrangian derivative $\mathrm{d}/\mathrm{d}t \equiv \partial_t + [\phi, .]$. $n$ and $\phi$ are the *total* normalized density and electric potential, and not only their fluctuating parts. In the SOL, the destabilizing density gradient is built up by the source term, namely by the ionization of recycling neutrals, and by the particle influx $S$ crossing the separatrix. Only the latter is retained here. Finally, the following normalization is adopted: $x = (r-a)/\rho_s$; $y = a\theta/\rho_s$; $t \to \Omega_s t$ and $(D,\nu) \to (D,\nu)\rho_s c_s$. Unless specified, typical numerical parameters are $\sigma_\parallel = 2.27 \times 10^{-4}$, $g = 5.72 \times 10^{-4}$, $D = 2 \times 10^{-2}$, with $\rho_s \approx 3.4 \times 10^{-4}$ m, $c_s \approx 9.8 \times 10^4$ $\mathrm{m\,s^{-1}}$ and $\Omega_s \approx 2.9 \times 10^8$ $\mathrm{s^{-1}}$. The box grid is $256 \times 256$, with $1\rho_s$ per grid point. Details on the numerical scheme can be found in [22]. The particle source is constant in time and poloidally (along $y$), with a Gaussian radial shape $S(x) = S_0 \exp[-(x/\lambda_s)^2]$, with $S_0 = 10^{-2}$ and $\lambda_s = L_x/30$. Such a treatment allows one to investigate two separate SOL regions: a stable one, where the density gradient and curvature have opposite signs, leading to a SOL width $\lambda_{\mathrm{SOL}}$ governed by collisional transport, and the turbulent region in which curvature and $\partial_x \bar{n}$ are colinear. The latter part is the turbulent SOL investigated in this paper.

### 2.2. Avalanches and SOL e-folding length

Most of the dynamical properties of the system described by Eq. (1) are discussed in a previous paper [14]. Basically, turbulent transport looks intermittent. It is dominated by long range transport events which seem to propagate almost ballistically when flux surface averaged. These bursts are called avalanches. Their effective velocity is a fraction of the acoustic speed in this model. More accurate 3D flux driven models exhibiting avalanche-like transport in the edge or core plasma report velocities of the order of a fraction of the ion diamagnetic drift $v_{*i} \approx \rho_* c_s$ [11,12]. Such dynamics can be understood either in terms of streamers, i.e. convective cells mainly elongated radially [8], or in terms of front propagation [7]. Both mechanisms are found to compete in non-linear simulations. It is worth noticing that radial transport velocities of a few $\mathrm{km\,s^{-1}}$ are also reported experimentally in the SOL [23,24].

A snapshot of the 2D density field is presented in Fig. 1. Poloidally localized 'fingers' appear to develop on a broad radial scale. Their complex structure, made of 'pitchfork' (stops) and 'mushroom' (goes) like shapes, reflects that of the underlying electric potential. Coupling between $n$ and $\phi$ comes from both the $E \times B$ advection velocity, and the curvature drift responsible for charge separation (term $g\partial_y \mathrm{Log}(n)$ in Eq. (1)). The strength of this coupling is all the larger since parallel current losses are small. Also, the dynamics and the shape of a given finger crucially depend on the pre-existing $\phi$ field it is propagating into. Analogously, the trajectory of an airplane can be dramatically modified by the wake of preceding ones. In that respect, the

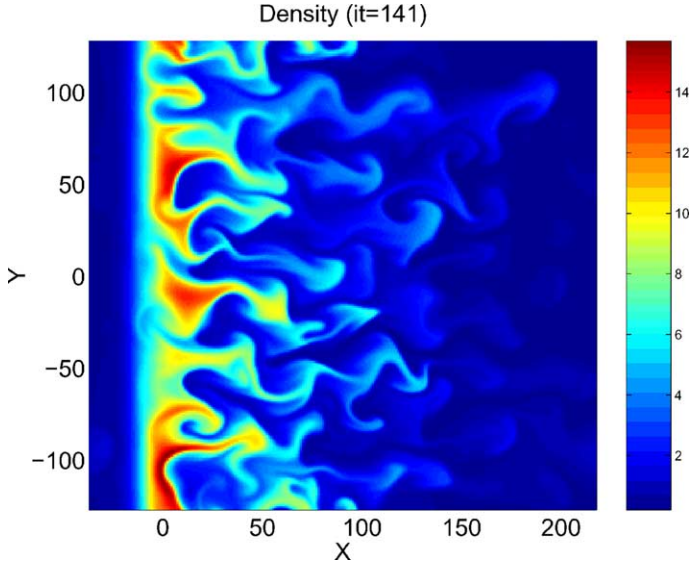


Fig. 1. Snapshot of the density field in the non-linear regime.

existence of blobs, as recently introduced to interpret experimental measurements, is questionable [25]. Our model suggest strong avalanches can be assimilated to blobs only for extremely weak coupling conditions (i.e. vanishing sheath conductivity), and providing that it can propagate a large radial distance without being stretched apart. This latter condition requires that its poloidal extent is smaller than the poloidal correlation length of turbulence, and that streamers are present. Additionally, as exemplified in the remainder of this paper, blobs are not necessary to account for the experimental observations.

The probability density function (PDF) of the radial flux at a given location $\Gamma(x_0, y_0, t) = -n\partial_y\phi$ is shown in Fig. 2. Note that $\Gamma$ can be negative, i.e. inwards. This is of particular importance for impurity transport. Depending on their poloidal injection location, they are liable to undergo fast inward transport up to the separatrix, similar to test particles. The PDF can be described by two distinct components: a Gaussian centered on zero – and hence of vanishing flux – and a log-normal distribution, accounting for the distribution tail which extends toward large outbursts. The Gaussian shape is expected to model the underlying diffusive-like transport, governed by both small-size turbulent eddies and the collisional transport associated with $D$. Surprisingly, the most probable equilibrium flux is negative. Such a decomposition of the PDF allows one to quantify the impact of rare but large events on the overall transport. In this case, it turns out that 44% of the total flux is carried out by events whose probability lies outside the $4\sigma$ domain. $\sigma$ refers here to the mean deviation of the Gaussian. The intermittent character is also reported experimentally [16,26,27].

Assuming Gaussian PDFs for both $\tilde{n}$ and $\tilde{\phi}$, the PDF of the flux is expected to exhibit asymmetric exponential tails. The asymmetry, allowing for a non-vanishing flux, is governed by the phase shift between the density and potential fluctuations [28]. Such a Gaussian condition is however not fulfilled in the 2D interchange turbulence studied here, since local density fluctuations $\tilde{n}$ are strongly non-Gaussian. It appears that the exponential asymmetry of the flux reflects both the cross correlation between $\tilde{n}$ and $\tilde{\phi}$, and avalanche events. Strikingly, Langmuir probe fluctuation measurements on Tore Supra exhibit similar characteristics [29].

The time averaged and instantaneous density profiles $\langle\bar{n}(x)\rangle$ and $\bar{n}(x, t_0)$, both recorded in the saturated phase of the non-linear regime, are shown in Fig. 3. The source profile is shown as well. Very steep density gradients can develop transiently. In Fig. 3, $\bar{n}$ exhibits a gradient length of the order of $10\rho_s$ at $x \approx 100$. In contrast, $\langle\bar{n}\rangle$ looks rather smooth, and exhibits an exponential decay although turbulent transport is not diffusive. Note, however, that a radial convective transport also leads to an exponential density profile. Should the parallel transport be balanced by convective turbulent transport of effective velocity $v_{\text{eff}}$, then the equilibrium time average density is exponential with an e-folding length of $\lambda_{\text{SOL}} = L_{\parallel} v_{\text{eff}}/c_s$. In the case presented in Fig. 3, the SOL e-folding length is of the order of $\lambda_{\text{SOL}} \approx 45\rho_s$ in the turbulent region, about 10 times larger than the one in the stable SOL, on the left hand side of the source. Turbulent activity can also lead transiently to very steep gradients, as exemplified in Fig. 3. Gradient lengths equal to the one generated by collisional transport develop locally. These gradient fronts are associated with avalanche-like events.

An important issue for fusion deals with the scaling of $\lambda_{\text{SOL}}$ with the driving flux $\Gamma_0 \equiv \int_0^{L_x} S(x)\,\mathrm{d}x$. Indeed, present day technical limitations of fusion devices include the limited capability of plasma facing components to extract a large amount of power. In that respect, spreading the outward power flux over a large

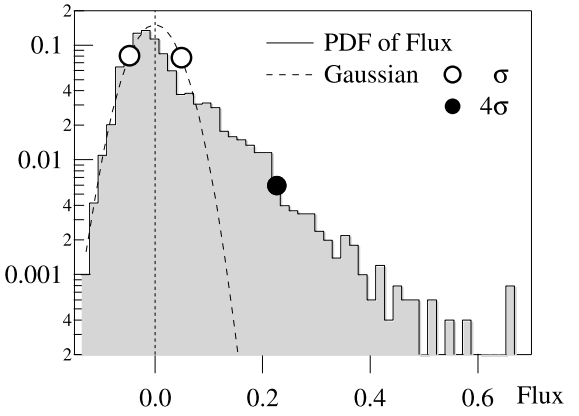


Fig. 2. PDF of the turbulent radial flux. A gaussian of vanishing mean flux fits the PDF of the inward flux (negative values).

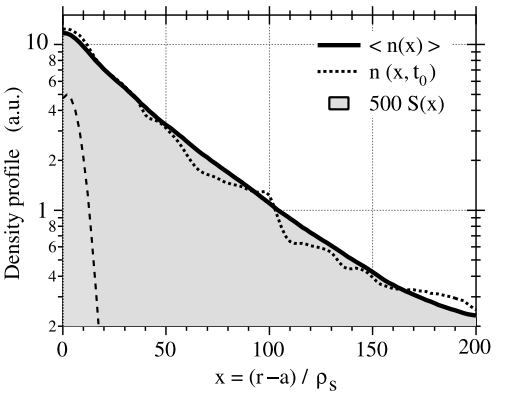


Fig. 3. Typical equilibrium (poloidally averaged) density profiles. Bold: time average; dashed line: at a given time.

region is highly beneficial. The dependence of $\lambda_{SOL}$ with $\Gamma_0$ has been investigated, all other parameters remaining unchanged. These numerical results have been obtained with the following set of normalized parameters: $g = 5 \times 10^{-4}$, $\sigma_{\|} = 10^{-5}$, $D = v = 5 \times 10^{-4}$, and a grid size equal to $64 \times 64$. The favorable point is the increase of $\lambda_{SOL}$ with $\Gamma_0$, which is thus potentially able to slightly reduce the thermal constraints on plasma facing materials. However, this increase remains weak: $\lambda_{SOL}$ only increases by a factor of about 2 when $S$ is multiplied by 80. Assuming a power law dependence would lead to $\lambda_{SOL} \sim S^{2/9}$. Such a result puts forward the crucial need for alternative means of controlling the SOL width $\lambda_{SOL}$.

### 2.3. Impact of viscosity on $\lambda_{SOL}$

The present paragraph investigates the sensitivity of $\lambda_{SOL}$ to the dissipative coefficients $(D, v)$, and more precisely to the viscosity. Theoretically, $v$ emerges from the anisotropy of the pressure tensor. In fluid codes, the viscosity coefficient $v$ appears as an ad hoc parameter. It is essential since it ensures the damping of small scale structures. It is usually assumed to have little or no impact on the code outputs since, generally, the turbulence generates a much larger diffusivity or viscosity.

However, in the framework of self-regulation of turbulence by ZF, the viscosity appears as a key parameter [30]. Indeed, numerous studies, both theoretical [31,32], numerical [6,12] and experimental [33,34] tend to show ZF govern the magnitude and dynamics of turbulent transport. Efficient ZF shearing tends to reduce the radial correlation of convective cells, hence lowering the transport [35]. Now, it also appears that ZF are damped by collisions and viscosity [36,37]. Especially, self-generated sheared flows can completely suppress turbulent transport in collisionless GK simulations of ITG modes run just above marginal stability [38]. More generally, any poloidal flow of poloidal extent larger than the underlying turbulence correlation length, and of lifetime longer than the turbulence correlation time, is likely to efficiently shear turbulent cells, possibly reducing the transport.

In the system described by Eq. (1), ZF are driven by the Reynolds stress. Linear damping of the mean poloidal velocity $\bar{v}_y$ is then ensured by the viscosity:

$$\partial_t \bar{v}_y \approx -\partial_x \overline{\tilde{v}_x \tilde{v}_y} + v \partial_{xx} \bar{v}_y.$$

Two simulations with low (L) and high (H) values of $v$ are compared: $v_L = 5 \times 10^{-3}$ and $v_H = 2 \times 10^{-2}$. $v_L$ is a typical value for the classical fluid viscosity due to ion–ion collisions. The enhanced value $v_H$ would stand for a charge exchange dominated viscosity, with neutral density reaching a tenth of the plasma density. So as to keep the linear properties the same, the diffusion coefficients are different as well: $D_L = v_H$ and $D_H = v_L$.

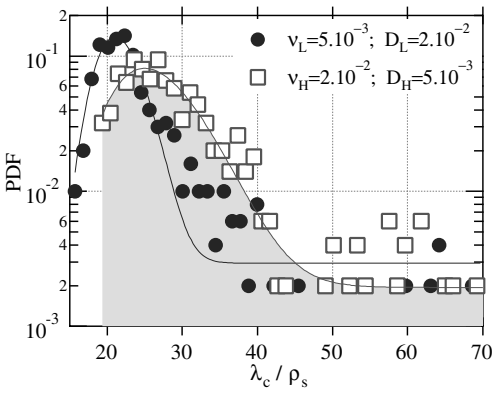


Fig. 4. PDF of the correlation length $\lambda_c$, as defined in the text, for $v_L = 5 \times 10^{-3}$ (circles) and $v_H = 2 \times 10^{-2}$ (squares). Solid lines are Log-normal distributions plotted 'to guide the eyes'.

An efficient way to quantify the difference between both simulations in the non-linear regime is to estimate the characteristic radial extent of convective cells at each time, $\lambda_c(t)$. This length is derived from the normalized 2D self-correlation function of the electric potential fluctuations, defined as $C_{\tilde{\phi}}(\Delta x, \Delta y, t) \equiv \langle \tilde{\phi}(x, y, t) \cdot \tilde{\phi}(x + \Delta x, y + \Delta y, t) \rangle_{x,y} / \langle \tilde{\phi}(x, y, t)^2 \rangle_{x,y}$. The points equal to $\frac{1}{2}$ form an ellipse centered on $(\Delta x, \Delta y) = (0, 0)$, whose largest diameter defines $\lambda_c$. $\lambda_c$ points essentially in the radial direction.

The larger $v$, the larger $\lambda_c$, as exemplified in Fig. 4. In the $v_H$ case, $\lambda_c$ exhibits very large transient excursions, almost covering the entire size of the system along the radial direction, reminiscent of streamers. Accordingly, the largest avalanches are observed in this simulation, where density fronts extend up to the very far SOL, namely $x > 100$. On average, $\lambda_c$ is 1.4 times larger for $v_H$ than for $v_L$. Consistently, turbulent transport is also increased. As a result, the density profile extends farther into the SOL with increasing $v$, leading to a larger (factor 1.4) SOL width $\lambda_{SOL}$. Defining an effective diffusivity $D_{eff} = -\langle \overline{\Gamma} \rangle / \langle \partial_x \bar{n} \rangle$, one finds $D_{eff}$ is larger by a factor of about 2.2 in the largest $v$ case. The exact role of ZF shearing in this change of transport magnitude is still to be investigated. This issue will be addressed in a future publication.

Noting that viscosity increases with collision frequency, the dependence of $\lambda_{SOL}$ with $v$ then allows one to expect the following: (i) the far SOL, characterized by a large amount of neutrals and a low temperature is likely to exhibit a large $\lambda_{SOL}$, in agreement with recent observations on DIII-D [39,40]. Also, (ii) $\lambda_{SOL}$ should decrease with increasing heating, i.e. at higher SOL temperature. The heat flux e-folding length is found to decrease with additional heating on Tore Supra [41]. Hence, the impact of viscosity on the size of convective cells and on the level of turbulent transport offers the

framework for a qualitative understanding of experimental evidence.

### 3. Measurements by a theoretical probe

A longstanding issue in edge turbulence measurements with a Langmuir probe deals with the impact of the diagnostic tool itself on the transport. In addition to plasma-surface interaction processes, the probe modifies locally the parallel current losses. Indeed, the probe collects or expels parallel current, depending on whether it is negatively (ion regime) or positively (electron regime) biased, respectively.

Linearly, parallel current losses $j_\parallel$ at the sheath are found to stabilize the interchange modes. Analytically, each poloidal mode of the parallel current is quadratic in phase with respect to that of the radial turbulent flux. As a consequence, if the phase shift between the fluctuating density and electric potential maximizes the radial transport, it will minimize the parallel current. This behavior is still observed in the non-linear regime of the simulations, where the particle radial flux $nv_{Ex}$ and $j_\parallel$ are nearly quadratic in phase, the extremum of one occurring at zeros of the other. The strong correlation between the cross-field radial transport and the parallel current loss at the end points of the field lines readily suggests that an external control of $j_\parallel$ might in turn modify the cross-field transport.

The present 2D model allows one to investigate this issue. In order to model the probe, the parameter $\Lambda$ is modified by an external control parameter, the probe biasing potential $V_{\text{bias}}$ [1,42]. This perturbation is localized both radially and poloidally, and has been given a Gaussian shape of characteristic width $\Delta_{\text{probe}}$: $V_{\text{bias}} \propto \exp\{-[(x-x_0)^2+(y-y_0)^2]/\Delta^2_{\text{probe}}\}$. The normalized parallel current then reads: $j_\parallel = n[1-\exp(\Lambda + V_{\text{bias}} - \phi)]$. In the limit $\Lambda + V_{\text{bias}} - \phi \to -\infty$, the probe works in the ion saturation current regime, the electron current is zero. This regime is achieved with $V_{\text{bias}} \to -\infty$ and allows one to measure the fluctuations of the ion saturation current in the case of fast data sampling (>10 kHz). Neglecting the fluctuations of the sound speed (readily related to temperature fluctuations), the fluctuation of the ion saturation current is then taken as a measure of the density fluctuations. In the present model at constant temperature, this is a working assumption. In the present model, both ends of the flux tube are biased similarly and the flute assumption imposes that the plasma potential $\phi$ remains constant along the field line. As a consequence, possible 3D effects cannot be accounted for. Especially, the turbulence associated with the Kelvin–Helmholtz instability which may develop close to plasma facing components [43] is out of reach of the present analysis. However, unless assuming that probe measurements are significantly affected by the turbulence generated by the probe itself, our model should capture the main physical ingredients involved in such experiments. Another shortfall of the flute assumption is to neglect parallel variations of mean fields such as the electric potential [44]. Such effects would be important if they would dominate the sheath parallel loss terms used in the model. However, this particular regime is not met in most experimental situations of interest. The flute assumption would then only affect the quantitative predictions of the model. The physics of the probe interaction with the background turbulence should thus be properly addressed in the present framework.

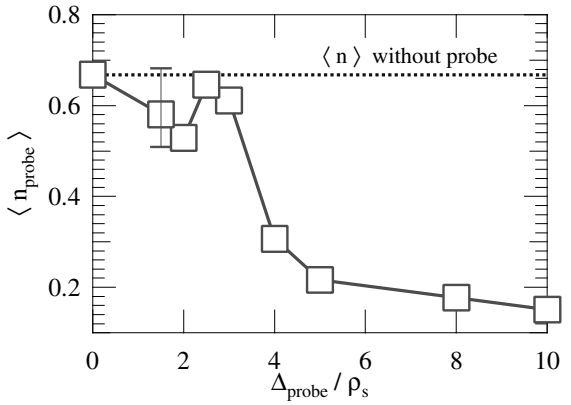


Fig. 5. Time averaged equilibrium density at the probe location as a function of the size of the probe $\Delta_{\text{probe}}$ ($V_{\text{bias}} = -5$). The horizontal dashed line refers to the value of $\langle \bar{n} \rangle$ in the absence of the probe.

The impact of the size of the probe $\Delta_{\text{probe}}$ on equilibrium density measurements is presented in Fig. 5. For these simulations, $D = \nu = 10^{-2}$, $S_0 = 5 \times 10^{-3}$ and $V_{\text{bias}} = -5$ is such that the probe is expected to operate in the saturation current regime ($\Lambda = +3.878$). On the contrary, the electron current is non-zero when the probe is large, leading to a *measured* mean density a factor of 4 smaller than the ambient one. This results from the strong response of the plasma potential to the perturbation at the probe position: $\phi_{\text{probe}} \approx \Lambda + V_{\text{bias}}$. In this case, a strong vorticity ring develops around the probe, which in turn screens the very center of the probe from avalanche-like transport. Consistently, the time evolution of the density at the probe is no longer bursty in this regime. On the basis of similar ideas, biasing of probes have been used to control the turbulent activity [45] or for larger probes, to trigger edge transport barriers [46] similar to those reported in the H-mode [47]. Possibly, 3D or kinetic effects could be advocated to reconcile large probe measurements with ambient turbulence in experiments. When $\Delta_{\text{probe}}$ is typically smaller than $3\rho_s$, $\phi_{\text{probe}}$ is roughly equal to $\Lambda$, such that the probe collects the ion saturation current.

The dynamics of density fluctuations are studied for $\Delta_{probe} = 1.5\rho_s$. It is compared to that of the density next to the probe. The Fourier spectra plotted in Fig. 6(a) exhibit the same shape, suggesting this particular statistical analysis captures the bursty character of the cross-field transport. However, Fig. 6(b) reveals that $\tilde{n}$ at the probe misses a significant number of large bursts. Indeed, the PDF at the probe exhibits a much smaller tail for large outbursts. Such a behavior goes along with the formation of a vortex structure around the probe, all the more efficient in screening the transport since $\Delta_{probe}$ is large.

Finally, the magnitude of the biasing potential is varied by steps to study the probe characteristics. $\Delta_{probe}$ is chosen equal to $1.5\rho_s$ so as to minimize the impact of the probe onto the ambient turbulence. $V_{bias}$ ranges from $-8$ in the ion regime ($j_{probe} = j_{sat}$) up to 5, i.e. in the electron regime. The resulting time averaged parallel current at the probe location is plotted in Fig. 7. The experimental characteristic is qualitatively recovered. Especially, $\langle j_{probe} \rangle$ saturates at $-j_{sat}$ in the ion regime, while it strongly increases for positive biasing. Also, the fluctuation magnitude around the mean value increases with $V_{bias}$, as indicated by the vertical 'error bars'. This behavior is attributed to the fact that positive biasing tends to focus avalanches onto the probe, leading to a significant enhancement of large bursts in this regime.

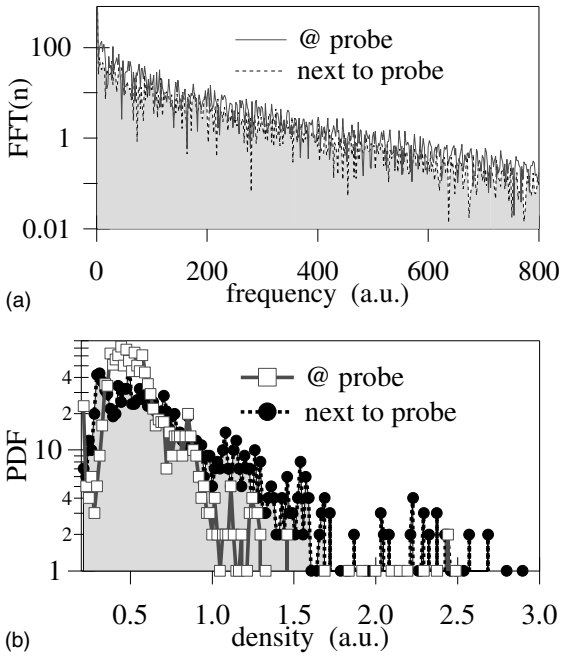


Fig. 6. (a) Fast fourier transform of the density at and next to the probe ($\Delta_{probe} = 1.5\rho_s$; $V_{bias} = -5$). (b) PDF of the density at and next to the probe ($\Delta_{probe} = 1.5\rho_s$; $V_{bias} = -5$).

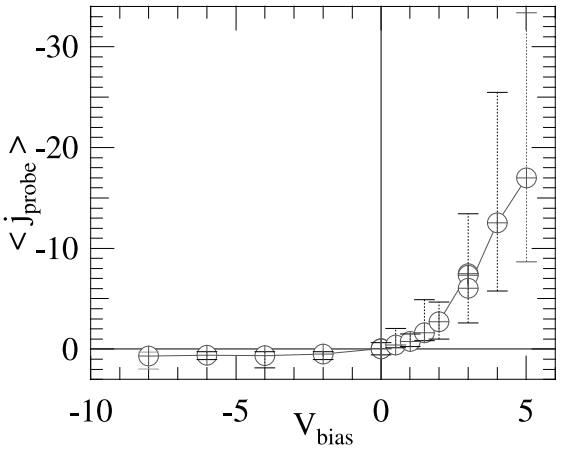


Fig. 7. Characteristics of the theoretical probe ($\Delta_{probe} = 1.5\rho_s$). Vertical 'error bars' refer to the magnitude of the fluctuations.

Such a property may render equilibrium density measurements at positive biasing particularly difficult.

## 4. Conclusion

Modeling of flux-driven 2D interchange turbulence in the SOL of fusion devices leads to bursty transport characterized by long range transport events, also called avalanches. These events are associated with radially elongated convective cells, which serve as channels for fronts of density gradient. These rare events are found to account for a significant part of the overall radial flux, in qualitative agreement with experiments, and lead to an exponential density profile. The resulting SOL e-folding length, $\lambda_{SOL}$, is found to increase very weakly with the magnitude of the driving flux. A power law dependence would yield a scaling of $S^{2/9}$. The impact of viscosity $\nu$ on turbulent transport is emphasized in this paper. Turbulent transport is found to increase with $\nu$, leading to a larger SOL width $\lambda_{SOL}$. It results from the increase of the characteristic size of convective cells along the radial direction. The exact role of ZFs in this shearing process is still to be determined. Probe measurements are also modeled by a spatially localized biased potential. For a too large extent of the theoretical probe, the plasma potential tends to follow the local perturbation, generating a vortex centered on the probe. This vortex acts as a shield for avalanches, leading to a significant drop of the mean density at the probe (factor 4). The ambient density is recovered for a sufficiently small probe. In this case, fluctuations exhibit a similar Fourier spectrum at and next to the probe, though the probe misses a significant number of large bursts. Finally, varying the biasing potential allows one to recover qualitatively the experimental probe characteristics, from the ion saturation regime up to the electron regime.

## References


[1] P.C. Stangeby, The plasma boundary of magnetic fusion devices, IOP, Bristol, 2000.
[2] G. Vayakis, AEA Fusion Report, vol. 123, 1991.
[3] J. Gunn, Phys. Plasmas 8 (2001) 1040.
[4] R. Mitteau, Ph. Chappuis, Ph. Ghendrih, A. Grosman, D. Guilhem, J. Gunn, J. Hogan, M. Lipa, G. Martin, J. Schlosser, E. Tsitrone, J. Nucl. Mater. 290–293 (2001) 1036.
[5] X. Garbet, L. Laurent, F. Mourgues, J.P. Roubin, A. Samain, in: Proceedings of the 12th IAEA Fusion Energy Conference, Nice, 1988, International Atomic Energy Agency, Vienna, Austria, 1989, vol. 2, p. 163.
[6] Z. Lin, T.S. Hahm, W.W. Lee, W.M. Tang, R.B. White, Science 281 (1998) 1835.
[7] Y. Sarazin, X. Garbet, Ph. Ghendrih, S. Benkadda, Phys. Plasmas 7 (2000) 1085.
[8] S. Champeaux, P.H. Diamond, Phys. Let. A 288 (2001) 214.
[9] P.H. Diamond, T.S. Hahm, Phys. Plasmas 2 (1995) 3640.
[10] B.A. Carreras, D. Newman, V.E. Lynch, P.H. Diamond, Phys. Plasmas 3 (1996) 2903.
[11] X. Garbet, R. Waltz, Phys. Plasmas 5 (1998) 2836.
[12] P. Beyer, S. Benkadda, X. Garbet, P.H. Diamond, Phys. Rev. Let. 85 (2000) 4892.
[13] A. Thyagaraja, Plasma Phys. Control. Fusion 42 (2000) B255.
[14] Y. Sarazin, Ph. Ghendrih, Phys. Plasmas 5 (1998) 4214.
[15] P.A. Politzer, Phys. Rev. Let. 84 (2000) 1192.
[16] M. Endler, H. Niedermeyer, L. Giannone, E. Holzhauer, A. Rudyj, G. Theimer, N. Tsois, ASDEX team, Nucl. Fusion 35 (1995) 1307.
[17] H.L. Berk, D.D. Ryutov, Yu. Tsidulko, Phys. Fluids B 3 (1991) 1346.
[18] X.Q. Xu, R.H. Cohen, Contrib. Plasma Phys. 36 (1998) 158.
[19] A.V. Nedospasov, Sov. J. Plasma Phys. 15 (1989) 659.
[20] X. Garbet, L. Laurent, J.-P. Roubin, A. Samain, Nucl. Fusion 31 (1991) 967.
[21] Ch.P. Ritz, R.V. Bravenec, P.M. Schoch, R.D. Bengtson, J.A. Boedo, J.C. Forster, K.W. Gentle, Y. He, R.L. Hickok, Y.J. Kim, H. Lin, P.E. Philips, T.L. Rhodes, W.L. Rowan, P.M. Valanju, A.J. Wootton, Phys. Rev. Let. 62 (1989) 1844.
[22] S. Benkadda, X. Garbet, A. Verga, Contrib. Plasma Phys. 34 (1994) 247.
[23] J. Boedo et al., these Proceedings.
[24] G. Counsell et al., these Proceedings.
[25] S.I. Krasheninnikov, Phys. Let. A 283 (2001) 368.
[26] C. Hidalgo, M.A. Pedrosa, B. van Milligen, E. Sanchez, R. Balbin, I. Garcia-Cortes, J. Bleuel, L. Giannone, H. Niedermeyer, Fusion Energy 1996, in: Proc. 16th Int. Conf. Montreal, 1996, vol. 1, IAEA, Vienna, vol. 617, 1997.
[27] G.Y. Antar, P. Devynck, X. Garbet, S.C. Luckhardt, Phys. Plasmas 8 (2001) 1612.
[28] B.A. Carreras, C. Hidalgo, E. Sánchez, M.A. Pedrosa, R. Balbin, I. Garcia-Cortés, B. van Milligen, D.E. Newman, V.E. Lynch, Phys. Plasmas 3 (1996) 2664.
[29] P. Devynck, private communication.
[30] M.A. Malkov, P.H. Diamond, Phys. of Plasmas 8 (2001) 3996.
[31] P.H. Diamond, M.N. Rosenbluth, F.L. Hinton, M. Malkov, J. Fleischer, A. Smolyakov, in: Proceedings of the 17th IAEA Fusion Energy Conference, Yokohama, 1998, International Atomic Energy Agency, Vienna, Austria, vol. 4, 1999, p. 1421.
[32] L. Chen, Z. Lin, R. White, Phys. Plasmas 7 (2000) 3129.
[33] S. Coda, M. Porkolab, K.H. Burrel, Phys. Rev. Let. 86 (2001) 4835.
[34] R.A. Moyer, G.R. Tynan, C. Holland, M.J. Burin, Phys. Rev. Lett. 87 (2001) 135001.
[35] T.S. Hahm, M.A. Beer, Z. Lin, G.W. Hammet, W.W. Lee, W.M. Tang, Phys. Plasmas 6 (1999) 922.
[36] M.N. Rosenbluth, F.L. Hinton, Phys. Rev. Let. 80 (1998) 724.
[37] B.N. Rogers, W. Dorland, M. Kotschenreuther, Phys. Rev. Let. 85 (2000) 5336.
[38] A.M. Dimits, T.J. Williams, J.A. Byers, B.I. Cohen, Phys. Rev. Let. 77 (1996) 71.
[39] R.A. Moyer et al., J. Nucl. Mater. 241–243 (1997) 633.
[40] J. Boedo et al., Rev. Sci. Instrum. 70 (1999) 2997.
[41] E. Tsitrone et al., in: Proc. 19th Symposium on Fusion Technology Portugal, 1996, p. 451.
[42] L. Tonks, I. Langmuir, Phys. Rev. 34 (1929) 876.
[43] X. Garbet, C. Fenzi, H. Capes, P. Devynck, G. Antar, Phys. Plasmas 6 (1999) 3955.
[44] V.A. Rozhansky, S.P. Voskoboynikov, E.G. Kaveeva, D.P. Coster, R. Schneider, Nucl. Fusion 41 (2001) 387.
[45] B. Richards, T. Uckan, A.J. Wootton, B.A. Carreras, R.D. Bengtson, P. Hurwitz, G.X. Li, H. Lin, W.L. Rowan, H.Y.W. Tsui, A.K. Sen, J. Uglum, Phys. Plasmas 1 (1994) 1606.
[46] R.R. Weynants, G. van Oost, G. Bertschinger, et al., Nucl. Fusion 32 (1992) 837.
[47] The ASDEX team, Nucl. Fusion 29 (1989) 1959.